

Mirror-induced reflection in the frequency domain

Yaowen Hu^{1,2,*}, Mengjie Yu^{1,3,*}, Neil Sinclair¹, Di Zhu¹, Rebecca Cheng¹, Cheng Wang⁴ and Marko Lončar^{1,†}

¹*John A. Paulson School of Engineering and Applied Sciences, Harvard University, Cambridge, MA 02138, USA*

²*Department of Physics, Harvard University, Cambridge, MA 02138, USA*

³*Ming Hsieh Department of Electrical and Computer Engineering, University of Southern California, Los Angeles, CA 90089, USA.*

⁴*Department of Electrical Engineering & State Key Laboratory of Terahertz and Millimeter Waves, City University of Hong Kong, Kowloon, Hong Kong, China*

**These authors contributed equally*

†Correspondence to: loncar@seas.harvard.edu

Mirrors are ubiquitous in optics and are used to control the propagation of optical signals in space. Here we propose and demonstrate frequency domain mirrors that provide reflections of the optical energy in a frequency synthetic dimension, using electro-optic modulation. First, we theoretically explore the concept of frequency mirrors with the investigation of propagation loss, and reflectivity in the frequency domain. Next, we explore the mirror formed through polarization mode-splitting in a thin-film lithium niobate micro-resonator. By exciting the Bloch waves of the synthetic frequency crystal with different wave vectors, we show various states formed by the interference between forward propagating and reflected waves. Finally, we expand on this idea, and generate tunable frequency mirrors as well as demonstrate trapped states formed by these mirrors using coupled lithium niobate micro-resonators. The ability to control the flow of light in the frequency domain could enable a wide range of applications, including the study of random walks, boson sampling, frequency comb sources, optical computation, and topological photonics. Furthermore, demonstration of optical elements such as cavities, lasers, and photonic crystals in the frequency domain, may be possible.

Synthetic dimensions, typically formed by a set of atomic [1,2] or optical modes [3–9], allow simulations of complex structures that are hard to do in real space, as well as high-dimensional systems beyond three-dimensional Euclidian space. Therefore, synthetic dimensions provide opportunities to investigate and predict, in a controlled manner, a wide range of physical phenomena occurring in e.g. ultracold atoms, solid state physics, chemistry, biology, and optics [3,10–12]. Exploration of synthetic dimension using optics has been of particular interest in recent decades, leveraging wide range of degrees of freedom of light, including space [4–6,13], frequency [14–25], time [9,26], and orbital angular momentum [24,27].

Integrated optics is an ideal platform for creating synthetic dimensions in the frequency domain, due to the high frequency and bandwidth of light, availability of strong nonlinear interactions, good stability and coherence of the modes, scalability, and excellent reconfigurability [11]. Furthermore, the ability to tailor the gain and loss within an optical system naturally allows the investigation of non-Hermitian physics which are typically hard to explore in other physical systems. Frequency synthetic dimensions in photonics has recently been experimentally investigated, including the measurement of band structure [14] and density of states of frequency crystals up to four dimensions [18], realization of two synthetic dimensions in one cavity [7], dynamical band structure measurement [15], topological windings [8] and braiding [28] in non-Hermitian bands, spectral long-range coupling [19], high-dimensional frequency conversion [21], frequency diffraction [16], and Bloch oscillations [17,29,30]. With a few exceptions [18,31], investigations of synthetic frequency dimensions on photonic chip have not been extensively studied. In particular, one of the most fundamental phenomena-- the reflection of light by synthetic mirrors -- has not been investigated yet in frequency synthetic dimensions.

Here we study, both theoretically and experimentally, reflection and interference of optical energy propagating in a discretized frequency space, i.e. one dimensional frequency crystal, caused by frequency-domain mirrors introduced in such a frequency crystal. The lattice points of the frequency crystal are formed by a set of frequency modes inside a thin-film lithium niobate (TFLN) micro-resonator, and the lattice constant is determined by the free spectral range (FSR) of the resonator (for a single spatial mode) [18]. Applying a continuous-wave (CW) electro-optic phase modulation to the optical resonator (Fig. 1a), at a frequency equal to the FSR (microwave-frequency range), results in coupling between adjacent frequency modes. Photons injected into such crystals can hop from one lattice site to another, leading to a tight-binding crystal [11,18]. The coupling strength between nearest neighbor lattice points, Ω , (Fig. 1b) is proportional to the voltage of the microwave driving signal and is related to the conventional modulation index β of a phase modulator as $\beta = 2\pi \frac{\Omega}{FSR}$ [32]. As a result, when injecting a CW optical signal into one of the crystal lattices sites (cavity resonances), optical energy spreads along the frequency synthetic dimension. A defect introduced in the frequency crystal can break the discrete translational symmetry of the lattice, resulting in reflection of light in the frequency domain (Fig. 1b). The defect can serve as a mirror in the frequency crystal, which is the frequency analog of the mirror in real space (Fig. 1c). The frequency mirror can be introduced by a mode splitting that is induced by coupling specific lattice points to additional frequency modes (Fig. 1d). These additional modes can be different spatial or polarization modes, clockwise and counterclockwise propagating modes of a cavity, or modes provided by additional cavities. In this work, we first use coupling between the traverse-magnetic (TM) and traverse-electrical (TE) modes to realize mirrors for the latter.

Then, we show that the frequency mirrors can also be realized using coupled resonators, an approach that allows better control, reconfigurability, and is more tolerant to fabrication imperfections.

We first theoretically investigate the frequency crystal dynamics for a reflection. For a conventional electro-optic frequency crystal without mirrors [18], the Hamiltonian is described by $H = \sum_{j=-N}^N \left(\omega_j a_j^\dagger a_j + \Omega \cos \omega_m t (a_j^\dagger a_{j+1} + h.c.) \right)$ in which a_j represents each frequency mode and ω_m is the modulation frequency that equal to the *FSR*. In the rotating frame of each mode $a_j \rightarrow a_j e^{-i(\omega_L + j\omega_m)t}$, they are all frequency-degenerate with a tight-binding coupling, i.e. $H = \sum_{j=-N}^N \left(\frac{\Omega}{2} (a_j^\dagger a_{j+1} + h.c.) \right)$. As a result, Lorentzian resonances of the resonator are broadened and have a profile corresponding to the density of states (DOS) of the crystal (Fig. 2a) [18]. Therefore, varying the laser detuning $\Delta = \omega_L - \omega_0$, where ω_L is the laser frequency and ω_0 is the 0th resonance of the resonator that the laser is pumping, changes the excitation energy ($E = \hbar\Delta$ in the rotating frame of the 0th resonance) of the pump signal (Fig. 2b, blue curve on the left side). This corresponds to the excitation of different modes of the band structure of the crystal (Fig. 2b, blue curve on the right side), leading to two synthetic Bloch waves with wave vectors k_\pm given by

$$k_\pm = \pm \frac{1}{a} \cos^{-1} \frac{\Delta}{\Omega}$$

in which $a = FSR$ is the lattice constant of the frequency crystal. For example, when $\Delta = 0$, two Bloch waves with wave vectors $k_\pm = \pm 0.5 \frac{\pi}{a}$ will be excited, representing waves that propagate along the positive and negative direction in frequency crystal (Fig. 3a) with a propagation phase of $\phi_p = k_\pm \times a = \pm 0.5\pi$ for a single hopping. To form a frequency mirror, additional mode b is used to break the periodic translation symmetry. We assume mode b (with a linewidth κ_b) is placed at frequency ω_{mr} that is frequency-degenerate with the crystal mode a_{mr} (with a linewidth κ) and the coupling strength between b and a_{mr} is μ . This additional mode b plays the role of the mirror with a reflection coefficient

$$r = - \frac{1 - \xi^2}{1 + \xi^2}$$

in which $\xi \approx -\frac{1}{1+(1+C)u}$. The parameter $C = 4\mu^2/\kappa_b\kappa$, analogous to the cooperativity in cavity quantum electrodynamics, is used to qualify the strength of the mirror ($C \sim 200$ in our work. See supplementary materials for details), and we assumed $u \equiv \frac{\kappa}{\Omega} \ll 1$ (see details in supplementary materials). This leads to interference between the forward propagating and the reflected waves (Fig. 1b) resulting in the final state

$$\psi(x) \sim e^{ikx} + r e^{ikx_{mr}} e^{-ik(x-x_{mr})}$$

where $k = k_\pm + i\frac{\alpha}{2}$, x_{mr} represents the position of the mirror, and α is related to the propagation loss of the Bloch wave in the frequency domain. The propagation loss $L = e^{-\alpha a}$ is defined as the power loss for a single hop and determined by the coupling strength Ω and linewidth of the resonator κ :

$$L \approx \left| \left(1 - \frac{u}{2} - \frac{u^2}{8} \right) \right|^2$$

In our TFLN platform we estimate the propagation loss L is 0.2 dB per lattice point with $u = 0.048$ (Fig. 2c), which is low enough to observe the interference and trapped state effects. With

the above expression for the final state $\psi(x)$, we show such interference causes an oscillation of energy distribution $|\psi(x)|^2$ along the frequency dimension and the oscillating period is determined by the wave vector k (Fig. 2d). Using the Heisenberg-Langevin equation, we numerically show that constructive/destructive interference in the frequency domain (see Supplementary Materials) leads to trapped states using multiple mirrors (Fig. 2e). The mirror provides a sharp cut-off to the propagation and a 20 dB power drop after passing the mirror.

The first approach we realize frequency domain mirrors based on polarization mode coupling inside a dispersion-engineered TFLN micro-resonator. This requires both refractive index and frequency degeneracy of TE-like and TM-like modes (from here on referred to as TE and TM modes, respectively) propagating inside the ring (Fig. 3a and 3b). The group index degeneracy provides large μ while frequency degeneracy leads to mode splitting. Due to the birefringence of lithium niobate, the TE modes that propagate along the y-direction and z-direction (of the thin-film lithium niobate crystal axes) have different indices $n_{o,TE}$ and $n_{e,TE}$ while the indices of TM modes are $n_{o,TM}$ for both directions. Therefore, by optimizing the cross-section of a x-cut lithium niobate micro-resonator, the value of $n_{o,TM}$ can be designed to be between the values of $n_{o,TE}$ and $n_{e,TE}$ over a broad range of wavelengths (Fig. 3c). When the TE mode circulates inside the micro-resonator, it experiences different averaged TE indices ranging from $n_{e,TE}$ to $n_{o,TE}$ at different bending points of the resonator. As a result, the TM modes can have an index degeneracy with the TE modes over a broad wavelength range (Fig. 3c). Frequency degeneracy was accomplished using a Vernier effect caused by the difference in FSR of TE and TM modes: the TM modes come in resonance with TE modes periodically, leading to periodic mode splitting that gives rise to periodic frequency mirrors (Fig. 3b). This coupling can be observed in the transmission spectrum of the TE modes (Fig. 3d).

To experimentally verify the presence and reflection of Bloch waves, we excite the frequency crystal at different values of detuning Δ . By pumping at $\Delta = 0$ on the device without mirrors (no polarization induced splitting) the energy propagates along the frequency dimension (Fig. 3e) without a reflection. However, when the device with engineered polarization-splitting is used, propagating wave is reflected by polarization-splitting induced mirror, and interference between the two waves leads to a constructive/destructive pattern at every other lattice points due to the propagation phase of $\phi_p = \pm 0.5\pi$. Note that the constructive interference results in a flat spectrum of generated comb signal which could be of interest for frequency comb applications. By varying the laser detuning Δ , we show varying interference fringes, due to the change of wave vector k (Fig. 3e).

Even better control of defects in the synthetic frequency dimension can lead to realization of frequency mirrors with controllable reflection strength and position in the crystal, as well as more complex arbitrary multi-mirrors configuration. Such control can be achieved in TFLN using the coupled-resonator platform (Fig. 4a). In our design, a long racetrack cavity (cavity 1) with a $FSR_1 = 10.5$ GHz is used to generate the frequency crystal through electro-optic modulation, while a small square-shaped cavity (cavity 2) with a $FSR_2 = 302.9$ GHz is coupled to the racetrack cavity to provide frequency mirrors through the resultant mode splitting. Interestingly, in our system, the coupling strength between two cavities μ can be larger than FSR_1 and as a result, a single resonance mode of the cavity 2 couples to multiple resonances of cavity 1 (Fig. 4b). This does not lead to a conventional two-mode-splitting but instead results in dispersive interactions that

gradually reduce FSR_1 in the frequency range around the resonances of cavity 2 (Fig. 4b). Indeed, the transmission spectrum of the device shows that the FSR_1 gradually varies from ~ 10.5 GHz to ~ 8.5 GHz and back to ~ 10.5 GHz in the wavelength around 1628.8 nm (Fig. 4c), corresponding to a 20% variation of the FSR_1 . To verify that this large change of FSR_1 originates from the formation of multi-hybrid modes due to the presence of cavity 2, we measured the wavelength-dependence of FSR_1 , and found that it is periodic with a period equal to FSR_2 (Fig. 4d). Finally, with the existence of multiple frequency mirrors, we verified the trapped state with constructive/destructive interference at every other lattice point in the coupled-resonator device (Fig. 4e). The strong mirror provides a cut-off of > 30 dB for the energy propagation in the frequency crystal. Despite the strong cut-off produced by the frequency mirrors, it is difficult to see multiple roundtrip effects within the two mirrors, due to the large propagation loss of our system (~ 0.2 dB/lattice point). Improving the quality factor of our TFLN rings $\sim 10^6$ (this work) to $\sim 10^7$ [33] and further improve the microwave driving power may lead to the realization of a frequency domain cavity [34]. The constructive/destructive interference redistributes the trapped optical energy within the two mirrors, which could be useful for frequency-specific engineering of the frequency spectrum, while avoiding energy leakage to other frequencies.

In summary, we have shown the reflection and trapped state of light in the frequency domain by introducing a mirror, that is, a defect, inside a frequency crystal. Our investigation utilizes the polarization mode-coupling and coupled-resonator both realized using the TFLN platform. We show the reflection and trapped state can be formulated as the reflection of Bloch waves due to defect scattering and be tuned by varying the wavevectors of Bloch waves. Introducing periodic mirrors via multiple-additional resonators with lower propagation loss may lead to the realization a frequency domain photonic crystal [35,36]. Furthermore, the ability to control the distribution of light in the frequency synthetic dimension provides an advantageous way to manipulate the light frequency. For example, the trapped state in the synthetic frequency crystal can be used to generate flat slope EO combs with better energy confinement in frequency domain, which is important for applications in spectroscopy, astronomy (astro-comb), and quantum frequency comb [37–41]. Finally, realizing frequency domain scattering beyond the reflection and transmission, using a high-dimensional frequency crystal [1,18,21,25] or other crystal structures [20,22], could pave ways to investigate high-dimensional geometrical phases and topologies. Our approach could form a basis for controlling the crystal lattice structure, band structure, and energy distributions in frequency domain.

Note added: In the process of writing this manuscript another group reported on the observation of frequency boundaries in the fiber-cavity system [42].

References

- [1] M. Lohse, C. Schweizer, H. M. Price, O. Zilberberg, and I. Bloch, *Exploring 4D Quantum Hall Physics with a 2D Topological Charge Pump*, Nature **553**, 55 (2018).
- [2] M. Mancini, G. Pagano, G. Cappellini, L. Livi, M. Rider, J. Catani, C. Sias, P. Zoller, M. Inguscio, M. Dalmonte, and L. Fallani, *Observation of Chiral Edge States with Neutral Fermions in Synthetic Hall Ribbons*, Science (80-.). **349**, 1510 (2015).
- [3] T. Ozawa and H. M. Price, *Topological Quantum Matter in Synthetic Dimensions*, Nat. Rev. Phys. **1**, 349 (2019).
- [4] A. Regensburger, C. Bersch, M. A. Miri, G. Onishchukov, D. N. Christodoulides, and U. Peschel, *Parity-Time Synthetic Photonic Lattices*, Nature **488**, 167 (2012).
- [5] E. Lustig, S. Weimann, Y. Plotnik, Y. Lumer, M. A. Bandres, A. Szameit, and M. Segev, *Photonic Topological Insulator in Synthetic Dimensions*, Nature **567**, 356 (2019).
- [6] O. Zilberberg, S. Huang, J. Guglielmon, M. Wang, K. P. Chen, Y. E. Kraus, and M. C. Rechtsman, *Photonic Topological Boundary Pumping as a Probe of 4D Quantum Hall Physics*, Nature **553**, 59 (2018).
- [7] A. Dutt, Q. Lin, L. Yuan, M. Minkov, M. Xiao, and S. Fan, *A Single Photonic Cavity with Two Independent Physical Synthetic Dimensions*, Science (80-.). **367**, 59 (2020).
- [8] K. Wang, A. Dutt, K. Y. Yang, C. C. Wojcik, J. Vučković, and S. Fan, *Generating Arbitrary Topological Windings of a Non-Hermitian Band*, Science (80-.). **371**, 1240 (2021).
- [9] C. Leefmans, A. Dutt, J. Williams, L. Yuan, M. Parto, F. Nori, S. Fan, and A. Marandi, *Topological Dissipation in a Time-Multiplexed Photonic Resonator Network*, Nat. Phys. **2104.05213**, (2022).
- [10] G. Semeghini, H. Levine, A. Keesling, S. Ebadi, T. T. Wang, D. Bluvstein, R. Verresen, H. Pichler, M. Kalinowski, R. Samajdar, A. Omran, S. Sachdev, A. Vishwanath, M. Greiner, V. Vuletić, and M. D. Lukin, *Probing Topological Spin Liquids on a Programmable Quantum Simulator*, Science (80-.). **374**, 1242 (2021).
- [11] L. Yuan, Q. Lin, M. Xiao, and S. Fan, *Synthetic Dimension in Photonics*, Optica **5**, 1396 (2018).
- [12] O. Boada, A. Celi, J. I. Latorre, and M. Lewenstein, *Quantum Simulation of an Extra Dimension*, Phys. Rev. Lett. **108**, 2 (2012).
- [13] S. Mittal, V. V. Orre, G. Zhu, M. A. Gorlach, A. Poddubny, and M. Hafezi, *Photonic Quadrupole Topological Phases*, Nat. Photonics **13**, 692 (2019).
- [14] A. Dutt, M. Minkov, Q. Lin, L. Yuan, D. A. B. Miller, and S. Fan, *Experimental Band Structure Spectroscopy along a Synthetic Dimension*, Nat. Commun. **10**, 1 (2019).
- [15] G. Li, Y. Zheng, A. Dutt, D. Yu, Q. Shan, S. Liu, L. Yuan, S. Fan, and X. Chen, *Dynamic Band Structure Measurement in the Synthetic Space*, Sci. Adv. **7**, 1 (2021).
- [16] C. Qin, F. Zhou, Y. Peng, D. Sounas, X. Zhu, B. Wang, J. Dong, X. Zhang, A. Alù, and P. Lu, *Spectrum Control through Discrete Frequency Diffraction in the Presence of Photonic Gauge Potentials*, Phys. Rev. Lett. **120**, 133901 (2018).
- [17] H. Chen, N. N. Yang, C. Qin, W. Li, B. Wang, T. Han, C. Zhang, W. Liu, K. Wang, H. Long, X. Zhang, and P. Lu, *Real-Time Observation of Frequency Bloch Oscillations with Fibre Loop Modulation*, Light Sci. Appl. **10**, (2021).
- [18] Y. Hu, C. Reimer, A. Shams-Ansari, M. Zhang, and M. Loncar, *Realization of High-Dimensional Frequency Crystals in Electro-Optic Microcombs*, Optica **7**, 1189 (2020).

- [19] B. A. Bell, K. Wang, A. S. Solntsev, D. N. Neshev, A. A. Sukhorukov, and B. J. Eggleton, *Spectral Photonic Lattices with Complex Long-Range Coupling*, *Optica* **4**, 1433 (2017).
- [20] Q. Lin, M. Xiao, L. Yuan, and S. Fan, *Photonic Weyl Point in a Two-Dimensional Resonator Lattice with a Synthetic Frequency Dimension*, *Nat. Commun.* **7**, 1 (2016).
- [21] K. Wang, B. A. Bell, A. S. Solntsev, D. N. Neshev, B. J. Eggleton, and A. A. Sukhorukov, *Multidimensional Synthetic Chiral-Tube Lattices via Nonlinear Frequency Conversion*, *Light Sci. Appl.* **9**, (2020).
- [22] D. Yu, G. Li, M. Xiao, D.-W. Wang, Y. Wan, L. Yuan, and X. Chen, *Simulating Graphene Dynamics in One-Dimensional Modulated Ring Array with Synthetic Dimension*, 1 (2021).
- [23] I. Martin, G. Refael, and B. Halperin, *Topological Frequency Conversion in Strongly Driven Quantum Systems*, *Phys. Rev. X* **7**, 1 (2017).
- [24] L. Yuan, Q. Lin, A. Zhang, M. Xiao, X. Chen, and S. Fan, *Photonic Gauge Potential in One Cavity with Synthetic Frequency and Orbital Angular Momentum Dimensions*, *Phys. Rev. Lett.* **122**, 83903 (2019).
- [25] T. Ozawa, H. M. Price, N. Goldman, O. Zilberberg, and I. Carusotto, *Synthetic Dimensions in Integrated Photonics: From Optical Isolation to Four-Dimensional Quantum Hall Physics*, *Phys. Rev. A* **93**, 043827 (2016).
- [26] H. Chalabi, S. Barik, S. Mittal, T. E. Murphy, M. Hafezi, and E. Waks, *Synthetic Gauge Field for Two-Dimensional Time-Multiplexed Quantum Random Walks*, *Phys. Rev. Lett.* **123**, 150503 (2019).
- [27] X. W. Luo, X. Zhou, C. F. Li, J. S. Xu, G. C. Guo, and Z. W. Zhou, *Quantum Simulation of 2D Topological Physics in a 1D Array of Optical Cavities*, *Nat. Commun.* **6**, 1 (2015).
- [28] K. Wang, A. Dutt, C. C. Wojcik, and S. Fan, *Topological Complex-Energy Braiding of Non-Hermitian Bands*, *Nature* **598**, 59 (2021).
- [29] N. R. A. Lee, M. Pechal, E. A. Wollack, P. Arrangoiz-Arriola, Z. Wang, and A. H. Safavi-Naeni, *Propagation of Microwave Photons along a Synthetic Dimension*, *Phys. Rev. A* **101**, 1 (2020).
- [30] C. Bersch, G. Onishchukov, and U. Peschel, *Experimental Observation of Spectral Bloch Oscillations*, *Opt. Lett.* **34**, 2372 (2009).
- [31] A. Balčytis, T. Ozawa, Y. Ota, S. Iwamoto, J. Maeda, and T. Baba, *Synthetic Dimension Band Structures on a Si CMOS Photonic Platform*, *Sci. Adv.* **8**, (2022).
- [32] Y. Hu, M. Yu, B. Buscaino, N. Sinclair, D. Zhu, A. Shams-Ansari, L. Shao, M. Zhang, J. M. Kahn, and M. Loncar, *High-Efficiency and Broadband Electro-Optic Frequency Combs Using Coupled Lithium-Niobate Microresonators*, *ArXiv* **2111.14743**, (2021).
- [33] M. Zhang, C. Wang, R. Cheng, A. Shams-Ansari, and M. Lončar, *Monolithic Ultra-High-Q Lithium Niobate Microring Resonator*, *Optica* **4**, 1536 (2017).
- [34] A. Yariv and P. Yeh, *Photonics: Optical Electronics in Modern Communications* (Oxford university press, 2007).
- [35] J. D. Joannopoulos, P. R. Villeneuve, and S. Fan, *Photonic Crystals: Putting a New Twist on Light*, *Nature* **386**, 143 (1997).
- [36] X. Lu, A. McClung, and K. Srinivasan, *High-Q Slow Light and Its Localization in a Photonic Crystal Microring*, *Nat. Photonics* **16**, 66 (2022).
- [37] N. Picqué and T. W. Hänsch, *Frequency Comb Spectroscopy*, *Nat. Photonics* **13**, 146 (2019).
- [38] L. Chang, S. Liu, and J. E. Bowers, *Integrated Optical Frequency Comb Technologies*,

- Nat. Photonics **16**, 95 (2022).
- [39] M. Kues, C. Reimer, J. M. Lukens, W. J. Munro, A. M. Weiner, D. J. Moss, and R. Morandotti, *Quantum Optical Microcombs*, Nat. Photonics **13**, 170 (2019).
- [40] N. C. Menicucci, S. T. Flammia, and O. Pfister, *One-Way Quantum Computing in the Optical Frequency Comb*, Phys. Rev. Lett. **101**, 1 (2008).
- [41] M. G. Suh, X. Yi, Y. H. Lai, S. Leifer, I. S. Grudin, G. Vasisht, E. C. Martin, M. P. Fitzgerald, G. Doppmann, J. Wang, D. Mawet, S. B. Papp, S. A. Diddams, C. Beichman, and K. Vahala, *Searching for Exoplanets Using a Microresonator Astrocomb*, Nat. Photonics **13**, 25 (2019).
- [42] A. Dutt, L. Yuan, K. Y. Yang, K. Wang, S. Buddhiraju, J. Vučković, and S. Fan, *Creating Boundaries along a Synthetic Frequency Dimension*, 1 (2022).

Acknowledgments: This work is supported by ARO/DARPA (W911NF2010248), NSF QuIC TAQS (OMA-2137723), DARPA TRAMPOLIN (HR0011-20-C-0137), AFRL Quantum Accelerator (FA9550-21-1-0056), ONR N00014-22-C-1041, NASA 80NSSC21C0583, NIH (5R21EY031895-02), Harvard Quantum Initiative, Research Grants Council, University Grants Committee (CityU 11212721)

Competing interests: M.L. are involved in developing lithium niobate technologies at HyperLight Corporation.

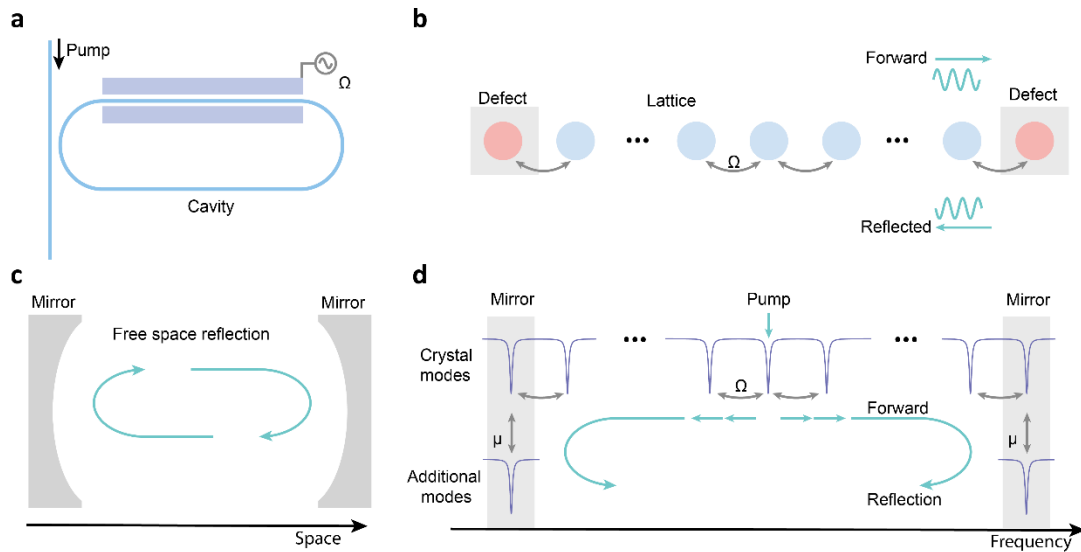


Fig. 1. Concept of the frequency mirror and mirror-induced reflection in the frequency crystal. **a**, Optical frequency crystals are generated using an optical resonator with electro-optic modulation. Microwave modulation, with frequency commensurate with the FSR of the resonator, creates nearest neighbor coupling Ω between adjacent frequency modes of the resonator. **b**, Defects introduced in the frequency crystal result in reflections of optical signal propagating in the synthetic frequency dimension. **c**, The reflection in frequency domain is analogous to the spatial reflection. **d**, Frequency mirror can be realized by coupling additional frequency modes to the crystal frequency modes. These additional modes will cause mode-splitting effect, thus breaking the periodic translational symmetry of the frequency crystal, creating effective reflections of light in frequency domain.

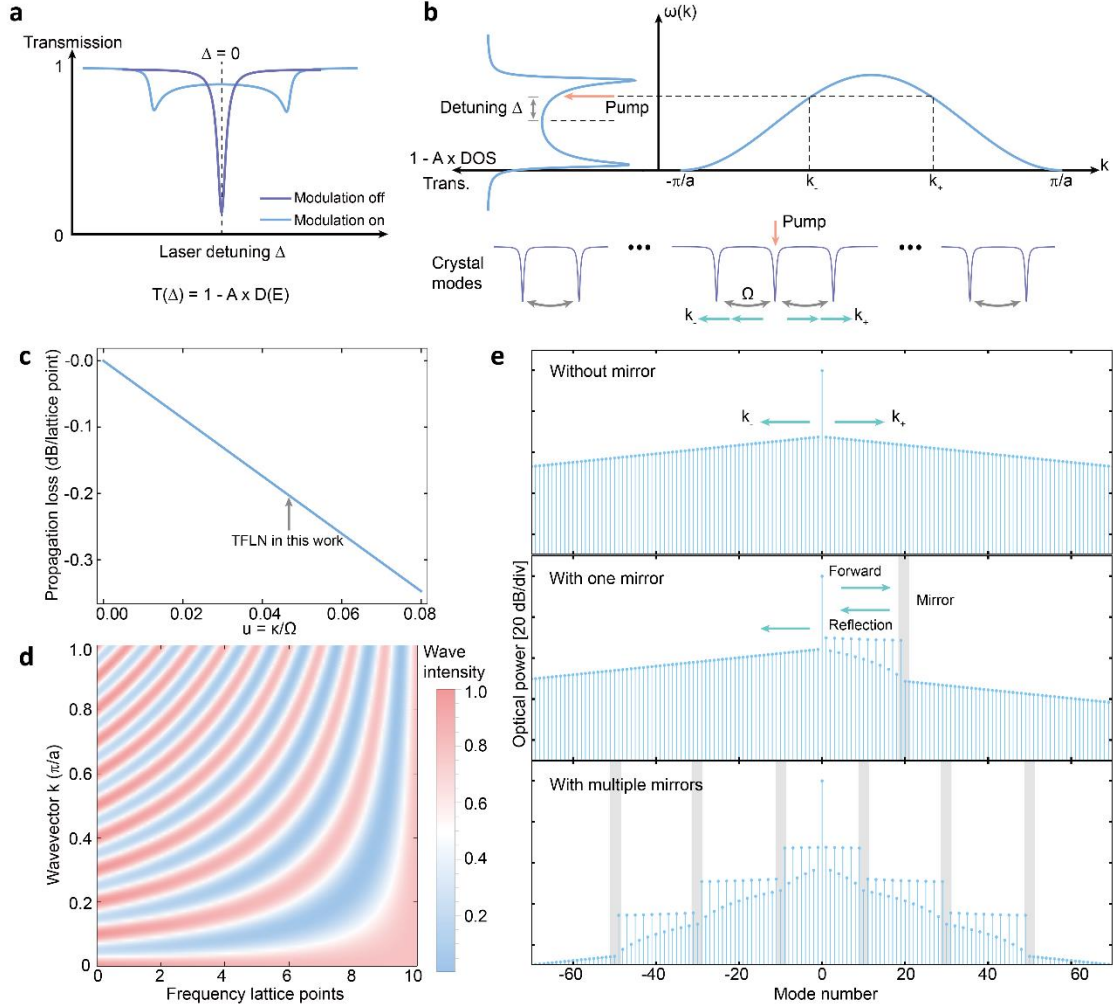


Fig. 2. Theory of the mirror-induced reflection and the trapped states in frequency domain. **a**, Illustration between the transmission spectrum of the resonator and density of states of the frequency crystal. When the modulation is off, the transmission shows a normal Lorentzian shape. When modulation is on, a frequency crystal is formed and each resonance is broadened. The transmission represents a direct link to the DOS, $T(\Delta) = 1 - A \times D(E)$, in which $T(\Delta)$ is the transmission, $D(E)$ is the DOS, and A represents a factor for DOS (see detailed form in [18]) **b**, With modulation on, the resonance shape corresponds to the density of states of the modes propagating in formed frequency crystal. Then, by controlling the laser detuning Δ , the wave vectors of the Bloch waves can be controlled. In the general case, detuning launches two Bloch waves propagating along the positive and negative direction of the frequency crystal, with wavevectors k_+ and k_- , respectively, as determined by the band structure of the crystal. **c**, Propagation loss of the energy inside the frequency crystal as a function of parameter $u = \kappa/\Omega$. **d**, Simulated energy distribution of the states that with a single frequency mirror using experimentally achieved values ($u = 0.048$, $C = 187$). The reflected wave interferes with the forwarded wave, forming constructive/destructive interference in the frequency domain. The period of the interference is determined by the wavevector. **e**, When there is no mirror in the frequency crystal

(top panel), the energy spreads through the EO modulation along the frequency dimension with a linear loss in dB scale. By applying one mirror, the Bloch waves are reflected, forming constructive/destructive interference (middle panel) with the optical energy located in every other lattice point enhanced/suppressed. When there are multiple mirrors, the light forms a trapped state in the frequency crystal (bottom panel), leading to flat spectrum for constructive interference in between mirrors.

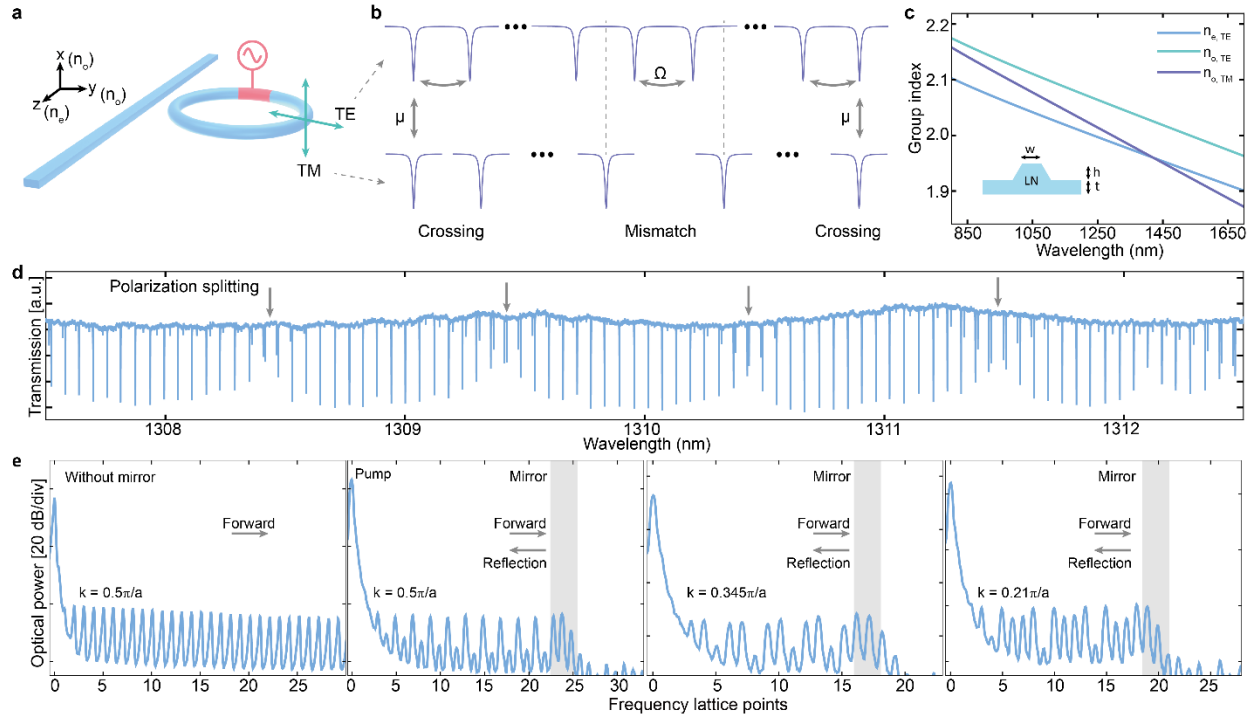


Fig. 3. Reflection induced interference in the frequency synthetic crystal using polarization coupling. **a**, On the x -cut thin-film lithium niobate, TE mode that propagates along the y - and z -direction has different indexes $n_{o,TE}$ and $n_{e,TE}$, while the TM mode has index of $n_{o,TM}$ for all directions. Dispersion engineering can be used to make the indices of TE and TM modes degenerate, leading to strong coupling μ between TE and TM resonances. **b**, The frequency mirrors induced by mode-splitting only happens when the TE and TM modes have both index and frequency degeneracy. Difference in FSR of TE and TM modes, guarantees that they frequency overlaps at some frequencies, leading to formation of periodic frequency mirrors. **c**, The group index $n_{o,TM}$ can be designed to be between the $n_{o,TE}$ and $n_{e,TE}$ via dispersion engineering. Then, TE mode circulating inside a x -cut lithium niobate resonator, it experiences different averaged indices (ranging from $n_{o,TE}$ to $n_{e,TE}$) at different bending points of the resonator. As a result, index degeneracy between TE and TM modes can be achieved over a broad wavelength range (850 nm to 1450 nm for $w = 1.4 \mu\text{m}$, $h = 350 \text{ nm}$, $t = 250 \text{ nm}$). **d**, Measured transmission spectrum of TE modes on the x -cut dispersion engineered lithium niobate device. The mode-splitting breaks the translation symmetry of the crystal, leading to frequency mirrors. **e**, Experimental verification of the reflection due to frequency mirror using polarization-crossing. Optical energy propagates along the frequency dimension when there is no mirror. Applying frequency mirror leads to interference states and varying the Bloch wavevectors can adjust the shape of the state. Due to the discrete nature of the crystal, our output signal measures the oscillation with a discrete sampling in frequency domain with a sampling period equal to the lattice constant. As a result, for $k = 0.5\pi/a$, the energy distribution on each lattice point shows constructive/destructive interference at every other lattice points. The patterns for $k = 0.345\pi/a$ and $k = 0.21\pi/a$ correspond to

different oscillation period compared to the case of $k = 0.5\pi/a$, leading to destructive interference at every three/four lattice points.

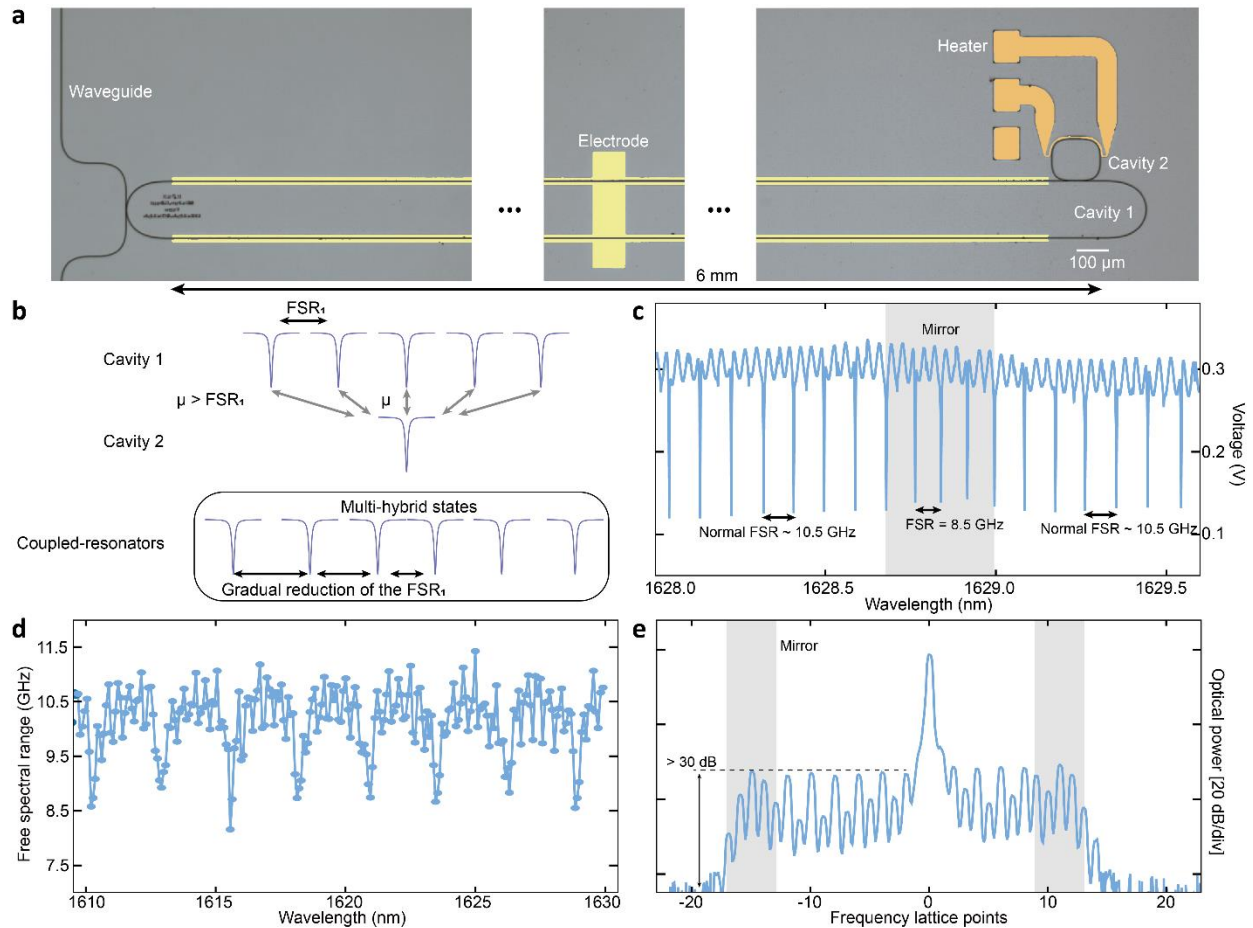


Fig. 4. Forming trapped states using frequency mirror implemented by coupled-resonators.

a, Optical image (false-color) of the device. A long racetrack shape cavity (cavity 1) with FSR₁ of 10.46 GHz is used to generate the frequency crystal. A rectangular shape (cavity 2) with FSR₂ of 302.9 GHz is coupled to the cavity 1 to provide the frequency mirrors. Metal electrodes (light yellow) provides the efficient microwave modulation. Thermal heater (orange) can tune the position of the mirrors by varying the resonances of cavity 2. **b**, Illustration of the coupling between two resonators when the coupling strength $\mu > \text{FSR}_1$. In this case, rather than having two-mode splitting of resonances of cavity 1, the single resonance of cavity 2 couples to multiple resonances of cavity 1, forming multi-hybrid modes and leading to a gradual reduction of FSR₁. **c**, Measured transmission spectrum of the device. The FSR₁ gradually changes from ~10.5 GHz (uncoupled value) to ~8.5 GHz and then goes back to ~10.5 GHz, indicating the strong coupling in presence of the resonance of cavity 2. **d**, FSR₁ as a function of wavelength. The FSR₁ features dips with periodicity equal to the FSR₂, thus confirming the strong coupling between the two cavities. **e**, Reflection at the mirror leads to constructive/destructive interference at every other lattice points. In addition, the mirror formed by coupling of multiple resonances supports trapped state, and provides > 30 dB suppression of transmitted optical energy.

Supplementary materials

Device fabrication

Our devices are fabricated from a commercial x-cut lithium niobate (LN) on insulator wafer (NANOLN), with a 600 nm LN layer, 2 μm buried oxide (thermally grown), on a 500 μm Si handle. Electron-beam lithography with hydrogen silsesquioxane (HSQ) resist followed by Ar^+ -based reactive ion etching (350 nm etch depth) are used to pattern the optical layer of the devices, including the rib waveguides and micro-ring resonators. The devices are cleaned, and microwave electrodes (15 nm of Ti, 300 nm of Au) are defined by photolithography followed by electron-beam evaporation and a bilayer lift-off process. One layer of SiO_2 (800 nm) using plasma-enhanced chemical vapor deposition (PECVD) is used to clad the devices. The heater (15 nm of Ti and 200 nm Pt) is defined by photolithography followed by electron-beam evaporation and lift-off. The heater is designed as a short metal strip (5 μm width) that is placed 3 μm away from the resonator on top of the SiO_2 cladding. The resistance of the heater is $\sim 140 \Omega$ (including parasitic resistance from routing strips). Tuning of the ring resonance by the FSR is achieved using a current of ~ 50 mA.

Measurement

Telecommunication-wavelength light from a fiber-coupled tunable laser passes through a polarization controller and is coupled to the LN chip using a lensed fiber. The output is collected using an aspheric lens and then sent to an optical spectrum analyzer (OSA) for characterization of the frequency components of the output signal. The microwave signal is generated from a synthesizer followed by a microwave amplifier and delivered to the electrodes on a device using an electrical probe.

Simulation of the frequency-mirror-induced reflection and the trapped states

Normal crystal dynamics without mirrors

We first consider the crystal dynamics without frequency mirrors. The optical frequency crystal generated using electro-optic modulation on a single cavity can be described by its Hamiltonian in the following form:

$$H = \sum_{j=-N}^N \omega_j a_j^\dagger a_j + \Omega \cos \omega_m t (a_j^\dagger a_{j+1} + h.c.)$$

where ω_j represents the frequency of each frequency mode, Ω is the coupling rate due to microwave modulation, and ω_m is the frequency of the microwave signal. The total number of frequency modes that are coupled are labelled by number -N to N. Using the Heisenberg-Langevin equation, we derived a set of equations of motion for each frequency mode a_j in the frequency crystal:

$$\dot{a}_j = \left(-i\omega_j - \frac{\kappa}{2}\right) a_j - i\Omega \cos \omega_m t (a_{j+1} + a_{j-1}) - \sqrt{\kappa_e} \alpha_{in} e^{-i\omega_L t} \delta_{j,0}$$

where the κ_e and κ are the coupling rate between the waveguide and cavity and the total loss rate of a_j , respectively. The pump power, frequency and pumped mode are denoted by α_{in} , ω_L and $\delta_{j,0}$, respectively. The frequency of each mode a_j is $\omega_j = \omega_0 + j \times FSR$ with ω_0 representing the 0th mode. Such a set of equations can be solved by changing the rotating frame for each mode $a_j \rightarrow a_j e^{-i\omega_L t} e^{-ij\omega_m t}$ and doing the Fourier transformation to solve this equation in frequency domain:

$$0 = \left(i\Delta + i\delta - \frac{\kappa}{2}\right) a_j - i\frac{\Omega}{2} (a_{j+1} + a_{j-1}) - \sqrt{\kappa_e} \alpha_{in} \delta_{j,0}$$

where $\delta = \omega_m - FSR$ and $\Delta = \omega_L - \omega_0$ are the microwave detuning and laser detuning, respectively.

Considering the case that $\Delta = \delta = 0$, we have the equation for each mode a_j

$$0 = -\frac{\kappa}{2}a_j - i\frac{\Omega}{2}a_{j+1} - i\frac{\Omega}{2}a_{j-1} - \sqrt{\kappa_e}\alpha_{in}\delta_{j,0}$$

We note that the equation of motion for the mode with largest mode number N is

$$0 = \left(-\frac{\kappa}{2}\right)a_N - i\frac{\Omega}{2}a_{N-1}$$

which leads to $a_N = -i\frac{\Omega}{\kappa}a_{N-1}$. As a result, the equation for a_{N-1} is

$$0 = \left(-\frac{\kappa}{2}\right)a_{N-1} - i\frac{\Omega}{2}a_{N-2} - \frac{\Omega}{2}\frac{\Omega}{\kappa}a_{N-1}$$

Therefore, we obtained another relation $a_{N-1} = -i\frac{\Omega}{\kappa(1+\frac{\Omega^2}{\kappa^2})}a_{N-2}$. By iterating the above steps, we obtain the relation for an arbitrary mode

$$a_l = -i\frac{\Omega}{\kappa} \frac{1}{1 + \frac{\frac{\Omega^2}{\kappa^2}}{1 + \frac{\frac{\Omega^2}{\kappa^2}}{1 + \frac{\frac{\Omega^2}{\kappa^2}}{1 + \frac{\kappa^2}{\dots}}}}} a_{l-1}$$

with the total number of the factor $\frac{\Omega^2}{\kappa^2}$ is $N - l$. As a result, the equation of motion for the 0th mode can be obtained as

$$0 = -\frac{\kappa}{2}a_0 - i\frac{\Omega}{2} \left(-i\frac{\Omega}{\kappa} \frac{1}{1 + \frac{\frac{\Omega^2}{\kappa^2}}{1 + \frac{\frac{\Omega^2}{\kappa^2}}{1 + \frac{\frac{\Omega^2}{\kappa^2}}{1 + \frac{\kappa^2}{\dots}}}}} a_0 - i\frac{\Omega}{2} \left(-i\frac{\Omega}{\kappa} \frac{1}{1 + \frac{\frac{\Omega^2}{\kappa^2}}{1 + \frac{\frac{\Omega^2}{\kappa^2}}{1 + \frac{\frac{\Omega^2}{\kappa^2}}{1 + \frac{\kappa^2}{\dots}}}}} a_0 - \sqrt{\kappa_e}\alpha_{in} \right) \right)$$

This equation is equivalent to

$$0 = \left(-\frac{\kappa}{2} - \frac{\kappa_{MW}}{2}\right)a_0 - \sqrt{\kappa_{e2}}\alpha_{in}$$

in which $\kappa_{MW} = \kappa \times 2(f_n - 1)$ with

$$f_n = 1 + \frac{\frac{\Omega^2}{\kappa^2}}{1 + \frac{\frac{\Omega^2}{\kappa^2}}{1 + \frac{\frac{\Omega^2}{\kappa^2}}{1 + \frac{\frac{\Omega^2}{\kappa^2}}{1 + \frac{\frac{\Omega^2}{\kappa^2}}{\dots}}}}}$$

In the limit of N is a very large number, we use the limit of $\lim_{n \rightarrow \infty} f_n = f$ and $f = 1 + \frac{\Omega^2}{f\kappa^2}$ to solve the final expression for f and κ_{MW} .

$$f = 1 + \frac{\frac{\Omega^2}{\kappa^2}}{1 + \frac{\frac{\Omega^2}{\kappa^2}}{1 + \frac{\frac{\Omega^2}{\kappa^2}}{1 + \frac{\frac{\Omega^2}{\kappa^2}}{\dots}}}} = \frac{1 + \sqrt{1 + \frac{4\Omega^2}{\kappa^2}}}{2}$$

$$\kappa_{MW} = \kappa \left(\sqrt{1 + \frac{4\Omega^2}{\kappa^2}} - 1 \right)$$

This κ_{MW} is the effective loss rate for the 0th mode that induced by the microwave modulation. With the expression of f , we can simplify the relation between a_l and a_{l-1} as

$$a_l = -i \frac{1}{uf} a_{l-1}$$

where $u \equiv \kappa/\Omega$ and $f = \frac{1 + \sqrt{1 + 4/u^2}}{2}$.

This gives the propagation loss:

$$L = e^{-\alpha a} \equiv \left| \frac{a_l}{a_{l-1}} \right|^2 = \left| \frac{1}{uf} \right|^2 = \frac{2}{u + 2\sqrt{1 + \frac{u^2}{4}}} \approx 1 - \frac{u}{2} - \frac{u^2}{8}$$

Frequency crystal with frequency mirrors

The frequency mirror can be introduced by coupling additional modes b_k ($k = 1, 2, \dots$) to the frequency crystal. To derive the reflection and transmission coefficient for the mirror, we consider a problem that a single additional mode b is coupled to a frequency mode a_{mr} with a coupling strength μ and b is frequency-degenerate with a_{mr} . Further, we consider the case that the pump source is far away from the mirror in frequency domain, i.e. the pump frequency is far away from the frequency of b . The equation of motions for a_{mr} and b are

$$\begin{aligned} 0 &= \left(-\frac{\kappa}{2}\right) a_{mr} - i \frac{\Omega}{2} (a_{mr+1} + a_{mr-1}) - i\mu b \\ 0 &= \left(-\frac{\kappa_b}{2}\right) b - i\mu a_{mr} \end{aligned}$$

Note that b is in a rotating frame of a_{10} since they are frequency degenerate. The steady-state solution of the above equations for each frequency mode and additional modes gives the simulated energy distribution of frequency crystals with mirrors (Fig. S1).

The mirror mode splits frequency space into two different regions: region that contains both input and reflected waves and the region that contains only the transmitted wave. Therefore, the region of frequency space that contains the transmitted wave should follow the normal dynamics of the frequency crystal, i.e. free propagation without reflection. As a result, we conclude that a_{mr} and a_{mr+1} will obey the relation

$$a_{mr+1} = -i \frac{1}{uf} a_{mr} \quad (1)$$

At the same time, we have the following equations:

$$0 = -\frac{\kappa}{2} a_{mr} - i \frac{\Omega}{2} a_{mr+1} - i \frac{\Omega}{2} a_{mr-1} - i\mu b \quad (2)$$

$$0 = \left(-\frac{\kappa_b}{2}\right) b - i\mu a_{mr} \quad (3)$$

With the equations (1), (2), and (3) we find

$$\frac{a_{mr+1}}{a_{mr-1}} = -\frac{1}{u^2 f(1+C)+1} \quad (4)$$

where $u \equiv \kappa/\Omega$, $f = \frac{1+\sqrt{1+4/u^2}}{2}$, and $C = 4\mu^2/\kappa_b\kappa$ is the parameter used to qualify the strength of the mirror.

For the region that contains both the input and reflected waves, due to the interference, we have

$$a_{mr-1} = (1+r) A_0 \quad (5)$$

where A_0 represents the input wave amplitude at the position of mirror.

The transmission and reflection coefficients are

$$t = \frac{a_{mr+1}}{A_0} \quad (6)$$

$$r^2 = 1 - t^2 \quad (7)$$

Using equation (4), (5), (6), and (7), the reflection coefficient is

$$r = -\frac{1 - \xi^2}{1 + \xi^2}$$

with $\xi = -\frac{1}{u^2 f(1+C)+1}$. In the regime that $u \ll 1$, we have $\xi \approx -\frac{1}{\left(u+\frac{u^2}{2}+\frac{u^3}{8}\right)(1+C)+1} \approx -\frac{1}{1+(1+C)u}$.

Finally, we have

$$R = |r|^2 = \frac{(1 - \xi^2)^2}{(1 + \xi^2)^2}$$

$$T = |t|^2 = \frac{4\xi^2}{(1 + \xi^2)^2}$$

To simulate the frequency crystal with arbitrary additional mirrors, i.e. several additional modes b_k ($k = 1, 2, \dots$) coupled to the crystal, we use the equation

$$\dot{a}_{mr,k} = \left(i\Delta + i\delta - \frac{\kappa}{2}\right) a_{mr,k} - i \frac{\Omega}{2} (a_{mr,k+1} + a_{mr,k-1}) - i\mu b_k$$

$$\dot{b}_k = \left(i\Delta + i\delta - \frac{\kappa}{2}\right) b_k - i\mu a_{mr,k}$$

where $a_{mr,k}$ is the mode that is frequency degenerate with b_k . We combine the above equations with the equations for modes that are not coupled to the mirrors

$$\dot{a}_j = \left(i\Delta + i\delta - \frac{\kappa}{2}\right) a_j - i\frac{\Omega}{2}(a_{j+1} + a_{j-1}) - \sqrt{\kappa_e} \alpha_{in} \delta_{j,0} \quad \text{for } j \neq k,$$

to numerically simulate the frequency crystals with mirrors.